Available online at www.sciencedirect.com
SCIENCE DIRECT
Geochimica et Cosmochimica Acta 70 (2006) 799–809
Geochimica
www.elsevier.com/locate/gca

Diffusion kinetics of Cr in olivine and ^{53}Mn–^{53}Cr thermochronology of early solar system objects

Motoo Ito [a,b], Jibamitra Ganguly [a,*]

[a] Department of Geosciences, University of Arizona, Tucson, AZ 85721, USA
[b] Radio Isotope Centre, University of Tokyo, 2-11-16 Yayoi, Bunkyo-Ku, Tokyo 113-0032, Japan

Received 5 May 2005; accepted in revised form 30 September 2005

Abstract

We have determined the diffusion coefficient of Cr in olivine as function of temperature, oxygen fugacity (fO_2), and crystallographic orientation and used these data to develop a quantitative understanding of the resetting of the short-lived ^{53}Mn–^{53}Cr decay system in olivine during cooling within meteorite parent body. The diffusion of Cr in olivine was found to be anisotropic, and effectively independent of fO_2 between wüstite–iron buffer and two orders of magnitude above this buffer. The diffusion data were used to calculate the spatially averaged mean closure temperature of the ^{53}Mn–^{53}Cr decay system in olivine as function of the initial temperature, cooling rate and grain size, and also the closure age profile of this system in olivine single crystal as function of radial distance and a dimensionless parameter that incorporates the effects of various parameters that affect the closure age. We also present a thermochronolgic formulation that permits retrieval of cooling rates from the extent of resetting of the bulk ^{53}Mn–^{53}Cr closure age of olivine during cooling. This method was applied to determine the cooling rate of the pallasite Omolon, which showed ^{53}Mn–^{53}Cr bulk age of olivine that is 10 Myr younger than the age of the solar system. The calculated cooling rate, which is 20–40 °C/Myr at ~985–1000 °C, is in good agreement with the metallographic cooling rate at ~500 °C, when the two results are considered in terms of a cooling model in which the reciprocal temperature increases linearly with time. The inferred cooling rate of Omolon, which seems to be a sample from the core-mantle boundary, yields a burial depth of ~30 km in a parent body of at least ~100 km radius.

1. Introduction

The ^{53}Mn–^{53}Cr decay system, with a half life of 3.7 Myr, has recently emerged as an important chronometer for the study of time scales of processes in the early history of the solar system when ^{53}Mn was still extant (e.g., Hutcheon et al., 1998; Lugmair and Shukolyukov, 1998; Nyquist et al., 2001; Sugiura, 2002). Excess ^{53}Cr relative to the terrestrial values has been detected in olivines, orthopyroxenes, spinels, and plagioclase from different types of meteorites (Hutcheon et al., 1998; Lugmair and Shukolyukov, 1998; Sugiura, 2002), and has led to the calculation of Mn–Cr mineral ages. The interpretation of these mineral ages requires quantitative understanding of the closure temperatures (T_c) below which there is no significant diffusive loss of the daughter products from a mineral. The T_c of a decay system in a given mineral, however, is not a unique quantity, but is a function of the grain size, cooling rate, and initial temperature of the mineral (Dodson, 1973; Ganguly and Tirone, 1999). Unambiguous formulation of T_c of the Mn–Cr system as function of these variables requires reliable experimental data on the diffusion parameters of Cr in the different minerals In addition, if these properties are known, one can calculate the cooling rate of the early solar system objects from the extent of resetting of ^{53}Mn–^{53}Cr mineral age, such as that reported by Lugmair and Shukolyukov (1998), using the extension of the classic Dodson formulation by Ganguly and Tirone (1999).

In this work, we report the experimental data on the diffusion kinetics of Cr in olivine, which constitutes a part of a comprehensive project on Cr diffusion in different minerals

* Corresponding author. Fax: +1 520 621 2672.
E-mail addresses: motoo@geo.arizona.edu (M. Ito), ganguly@geo.arizona.edu (J. Ganguly).

0016-7037/$ - see front matter © 2005 Elsevier Inc. All rights reserved.
doi:10.1016/j.gca.2005.09.020

in which excess radiogenic Cr (Cr*) has been detected in meteorite samples. We then use these data to calculate the T_c of the Mn–Cr decay system in olivine and also formulate a thermo-chronometer that can be used to calculate the cooling rate, in an absolute time frame, from the extent of resetting of Mn–Cr age of olivine. Finally, we apply the new thermo-chronometer to calculate the cooling rate of a pallasite, Omolon, to address the problem of cooling rates of this class of meteorites.

2. Experimental method

2.1. Starting material

For diffusion kinetic experiments, we used gem-quality natural olivine crystals, Fo_{91}, from San Carlos, Arizona. The Cr content of the crystals is less than 0.02 wt%. Full chemical analysis of a representative grain, as determined by an electron microprobe (Cameca SX50), is given in Table 1. The crystals were chemically homogeneous, and were carefully selected to be free of inclusions and internal cracks under an optical microscope.

Since the diffusion in olivine is, in principle, anisotropic because of its orthorhombic symmetry, and earlier studies showed significant anisotropy of cation diffusion (e.g., Buening and Buseck, 1973; Misener, 1974; Morioka and Nagasawa, 1991; Chakraborty et al., 1994), we oriented the selected crystals in an X-ray diffractometer to identify the directions of the *a*, *b*, and *c* crystallographic axes, which are also the directions of its principal diffusion axes. (The flux along a principal diffusion axis depends only the diffusion coefficient, *D*, and concentration gradient along that axis, and determination of *D* along the three principal diffusion axes of a mineral permit calculation of *D* along any arbitrary axis (e.g., Crank, 1975).) Sections were cut normal to the *a*- and *c*-crystallographic directions, and polished stepwise down to 0.25 μm diamond powder and finally finished, following Ganguly et al. (1998a), to a mirror-polish by a combination of chemical and mechanical polishing (2–3 min at 200 rpm) using silica suspension on OP-chem cloth from Struers. The last step was intended to remove a very thin disturbed layer that usually develops very close to a crystal surface after the mechanical polishing. The presence of a disturbed layer was indicated by etching the surface with 1 N HCl after polishing with 0.25 μm diamond, which led to the development of etch marks. To ensure that this weak layer was removed by the combination of chemical and mechanical polishing, one sample was tested by etching with the same solution. Examination of the sample under an optical microscope did not show any etch pattern.

Table 1
Electron probe data (average of 5 analyses) of San Carlos olivine used in the diffusion study

Oxide	wt% (1σ)		Atom proportion (1σ)
Na_2O	0.0461 (0.0256)	Na	0.0022 (0.0012)
K_2O	0.0048 (0.0042)	K	0.0001 (0.0001)
FeO	8.4622 (0.0963)	Fe	0.1712 (0.0021)
SiO_2	40.8655 (0.4231)	Si	0.9885 (0.0041)
MgO	50.8762 (0.1269)	Mg	1.8347 (0.0076)
CaO	0.0748 (0.0063)	Ca	0.0019 (0.0002)
Al_2O_3	0.0177 (0.0098)	Al	0.0005 (0.0003)
Cr_2O_3	0.0181 (0.0119)	Cr	0.0003 (0.0002)
MnO	0.1209 (0.0050)	Mn	0.0025 (0.0001)
TiO_2	0.0137 (0.0195)	Ti	0.0002 (0.0004)
NiO	0.3723 (0.0403)	Ni	0.0072 (0.0007)
Total	100.8723 (0.5899)	Cations	3.0095 (0.0046)
Fo[a]	91	Oxygen	4.00

[a] $Fo = 100 \times Mg/(Mg + Fe + Cr + Mn + Ni + Ca)$.

2.2. Tracer diffusion experiments

All experiments were carried out in a vertical gas mixing furnace at controlled fO_2 condition that was imposed by computer controlled flowing mixture of CO and CO_2. The experimental conditions are summarized in Table 2. The polished sections of olivine were thermally pre-annealed for 24 h at 900 °C and fO_2 condition corresponding to that of wüstite–iron (WI) buffer. The purpose of pre-annealing was to equilibrate the point defect structure of the crystals to a condition that is close to the experimental conditions, and also to anneal the surface defects that might have been generated by the polishing process.

A thin layer of Cr, ~200–250 Å, was deposited on the polished surface of a pre-annealed crystal by thermal evaporation of Cr_2O_3 under a high vacuum condition. In order to induce a diffusion profile, a sample with thin surface layer of Cr was annealed at a temperature between 900 and 1100 °C at 1 bar for a desired length of time under controlled fO_2 condition with a flow rate of CO–CO_2 mixture of ~200 cm^3/min. A zirconia sensor, with the reference junction at fO_2(air), was used to monitor the fO_2(CO–CO_2 mixture) continuously during diffusion experiments. The fO_2 condition that was intended to be imposed by the CO–CO_2 mixture agreed almost exactly with that monitored by the emf of the sensor. Fresh air was continuously pumped into reference junction during the course of an experiment. To determine the Arrhenian relation, the fO_2 of the experiments were controlled to those of WI buffer. Two orders of magnitude higher fO_2 conditions were imposed in three experiments to determine the effect of fO_2 on the Cr diffusion coefficient. This is the maximum fO_2 condition that can be imposed in our furnace stemming from the maximum attainable flow rate of CO_2 of 380 cm^3/min. The thickness of the surface layer at the end of diffusion anneals was estimated to be within 20–30 Å.

2.3. Measurements of diffusion profiles

The experimental diffusion profiles of ^{52}Cr in the olivine, along with the variations of ^{26}Mg, ^{30}Si, ^{52}Cr, ^{56}Fe, and ^{197}Au were analyzed by depth profiling in an ion microprobe (Cameca, ims-3f SIMS at Arizona State University),

Table 2
Summary of experimental conditions and Cr diffusion coefficients in olivine

T (°C)	Run #	Time (h)	D ($m^2\ s^{-1}$)	Log D ($m^2\ s^{-1}$)	Log fO_2 (bars)
Diffusion direction: ‖ *c*-axis					
900	CrOl90#1	24	$8.06\ (\pm2.76)\times10^{-21}$	-20.09 ± 0.15	−20.80 (WI)[a]
	CrOl90#1	24	$9.97\ (\pm2.15)\times10^{-21}$	-20.00 ± 0.09	−20.80 (WI)
	CrOl90#1	24	$1.00\ (\pm0.26)\times10^{-20}$	-20.00 ± 0.11	−20.80 (WI)
	CrOl90#2	72	$9.54\ (\pm2.27)\times10^{-21}$	-20.02 ± 0.10	−20.80 (WI)
	CrOl90#2	72	$1.13\ (\pm0.39)\times10^{-20}$	-19.95 ± 0.15	−20.80 (WI)
950	CrOl95#1	50	$6.40\ (\pm0.97)\times10^{-20}$	-19.19 ± 0.07	−18.29 (WI)
	CrOl95#1	50	$6.00\ (\pm1.05)\times10^{-20}$	-19.22 ± 0.08	−18.29 (WI)
1000	CrOl1k#1	4	$1.26\ (\pm0.28)\times10^{-19}$	-18.90 ± 0.10	−16.19 (WI)
	CrOl1k#1	4	$1.08\ (\pm0.32)\times10^{-19}$	-18.96 ± 0.13	−16.19 (WI)
	CrOl1k#2	8	$1.78\ (\pm0.11)\times10^{-19}$	-18.75 ± 0.03	−16.19 (WI)
	CrOl1k#3	16	$1.40\ (\pm0.05)\times10^{-19}$	-18.85 ± 0.02	−16.19 (WI)
	CrOl1k#4	48	$1.46\ (\pm0.11)\times10^{-19}$	-18.84 ± 0.03	−16.19 (WI)
	CrOl1k#4	48	$8.53\ (\pm0.91)\times10^{-20}$	-19.07 ± 0.05	−16.19 (WI)
1050	CrOl105#1	3	$2.37\ (\pm0.23)\times10^{-19}$	-18.62 ± 0.04	−14.42 (WI)
	CrOl105#1	3	$2.28\ (\pm0.26)\times10^{-19}$	-18.64 ± 0.05	−14.42 (WI)
	CrOl105#1	3	$2.59\ (\pm0.30)\times10^{-19}$	-18.59 ± 0.05	−14.42 (WI)
1100	CrOl110#1	0.5	$1.16\ (\pm0.36)\times10^{-18}$	-17.94 ± 0.14	−12.90 (WI)
	CrOl110#1	0.5	$1.20\ (\pm0.32)\times10^{-18}$	-17.92 ± 0.11	−12.90 (WI)
1000	Cr1k#1@hO	10	$7.97\ (\pm1.31)\times10^{-20}$	-19.10 ± 0.07	−14.19 (WI + 2)[b]
	Cr1k#1@hO	10	$9.74\ (\pm1.27)\times10^{-20}$	-19.01 ± 0.06	−14.19 (WI + 2)
	Cr1k#1@hO	10	$1.03\ (\pm0.12)\times10^{-19}$	-18.99 ± 0.05	−14.19 (WI + 2)
	Cr1k#2@hO	10	$1.01\ (\pm0.14)\times10^{-19}$	-19.00 ± 0.06	−14.19 (WI + 2)
	Cr1k#2@hO	10	$1.00\ (\pm0.08)\times10^{-19}$	-19.00 ± 0.03	−14.19 (WI + 2)
1100	Cr11#1@hO	0.5	$1.47\ (\pm0.06)\times10^{-18}$	-17.83 ± 0.02	−10.90 (WI + 2)
	Cr11#1@hO	0.5	$1.32\ (\pm0.08)\times10^{-18}$	-17.88 ± 0.03	−10.90 (WI + 2)
	Cr11#1@hO	0.5	$1.39\ (\pm0.08)\times10^{-18}$	-17.86 ± 0.02	−10.90 (WI + 2)
Diffusion direction: ‖ *a*-axis					
1000	CrOl1k_a#1	8	$2.04\ (\pm0.14)\times10^{-20}$	-19.69 ± 0.03	−16.19 (WI)
	CrOl1k_a#1	8	$1.87\ (\pm0.10)\times10^{-20}$	-19.73 ± 0.02	−16.19 (WI)
	CrOl1k_a#1	8	$1.51\ (\pm0.15)\times10^{-20}$	-19.82 ± 0.04	−16.19 (WI)
1050	CrOl105_a#1	10	$7.63\ (\pm0.88)\times10^{-20}$	-19.12 ± 0.05	−14.42 (WI)
	CrOl105_a#1	10	$7.11\ (\pm0.93)\times10^{-20}$	-19.15 ± 0.06	−14.42 (WI)
	CrOl105_a#1	10	$6.40\ (\pm0.49)\times10^{-20}$	-19.19 ± 0.03	−14.42 (WI)
1100	CrOl110_a#1	0.5	$1.92\ (\pm0.15)\times10^{-19}$	-18.72 ± 0.03	−12.90 (WI)
	CrOl110_a#1	0.5	$2.11\ (\pm0.13)\times10^{-19}$	-18.68 ± 0.03	−12.90 (WI)
	CrOl110_a#1	0.5	$2.16\ (\pm0.14)\times10^{-19}$	-18.67 ± 0.03	−12.90 (WI)

[a] WI, fO_2 condition corresponding to that of wüstite–iron buffer.
[b] WI+2, fO_2 condition two orders of magnitude higher than WI buffer.

following the procedure described by Ito and Ganguly (2004) (Fig. 1). The primary ion beam was mass-filtered negative ^{16}O accelerated to 10 keV with a beam current of 30–80 nA. The beam spot size was ~30–70 μm in diameter. The samples were held at +4.5 kV resulting in an impact energy of 14.5 keV. The primary ion beam was rastered over $\sim125\times125$ μm square area during analyses. Electrostatic charging of a sample by the primary ion beam was virtually eliminated by a gold film of 30 nm thicknesses that was evaporated on the sample surface prior to the analyses.

The positive secondary ions of ^{26}Mg, ^{30}Si, ^{52}Cr, ^{56}Fe, and ^{197}Au were monitored during the sputtering. By using mechanical aperture, only the secondary ions from the central 60 μm diameter of the rastered area were collected during the depth profiling. To eliminate interference by molecular ions, an offset of −75 V was applied to the sample voltage. Analyses of ^{197}Au, which was deposited on the crystal surface as a thin conducting film for the SIMS analyses, helped locate the crystal surface, whereas the concentration profiles of the non-diffusing species ^{30}Si and ^{56}Fe allowed us to monitor the stability of the analyses (Ito

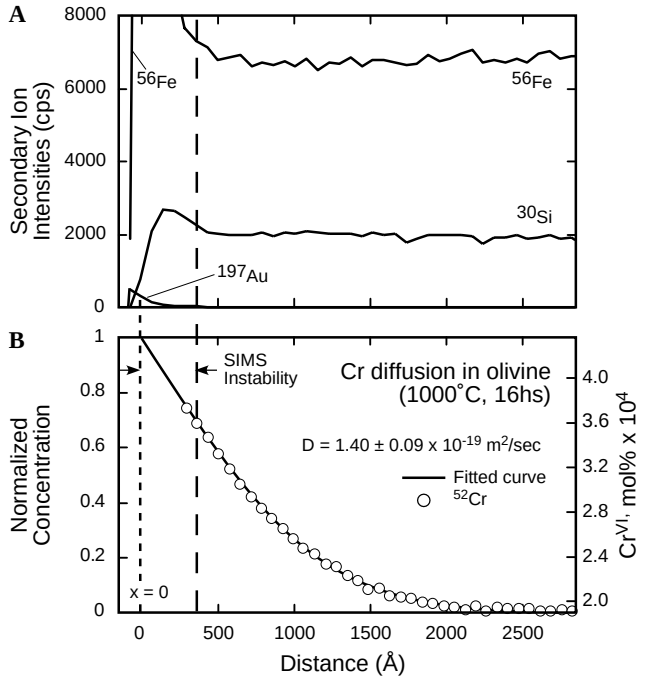

Fig. 1. Typical SIMS depth profile of ^{52}Cr parallel to the *c*-axis in olivine, which was annealed for 16 h at 1 bar, 1000 °C at fO_2 of WI buffer, along with those of ^{30}Si, ^{56}Fe, and ^{197}Au. The crystal surface ($x = 0$) was located to coincide with the depth at which the intensity of ^{197}Au reduced to half the peak value, whereas the depth of nearly simultaneous stabilization of ^{30}Si, ^{56}Fe were used to determine the initial analytical cycles of instrumental instability. The model fit to the ^{52}Cr data, according to the homogeneous infinite source model, is shown by solid line.

and Ganguly, 2004). Plateau intensities of the non-diffusing species were achieved after a few measurement cycles, as seems to be typical for SIMS analyses. The data for ^{52}Cr were ignored for these initial measurement cycles. Crater depths were determined with a TENCOR surface profilometer, which was calibrated against known standards. The crystal surface ($x = 0$) below the thin film was located on the basis of the intensity of ^{197}Au signal, assuming that it was coincident with the depth-profiling step where the intensity of this signal was reduced to half its peak value.

3. Results and discussion

A typical diffusion profile of ^{52}Cr parallel to the *c*-axis of olivine, and a model fit to the data, are shown in Fig. 1B. The model fit was calculated according to the solution of the diffusion equation, in cartesian coordinates, for diffusion of species into a semi-infinite medium from an infinite source (Crank, 1975), The solution is

$$\frac{C_s - C(x,t)}{C_s - C_\infty} = \mathrm{erf}\left(\frac{x}{2\sqrt{Dt}}\right), \quad (1)$$

where x is the distance from the interface, t is the time, and $C_\infty = C$ at $t = 0$ and $x = \infty$. Since C_s could not be measured directly due to the initial instability of the ion beam (Fig. 1), we solved for both D and C_s, following Ganguly et al. (1998b), by interfacing the above solution to an optimization program, MINUIT (James and Roos, 1975). In addition to the above solution of the diffusion equation, we also tried the solution for a depleting source (Crank, 1975, Eq. 2.6), optimizing it with MINUIT, but the solution for the infinite source yielded better fit to the experimental data than the depleted source model in all cases. The D values calculated according to Eq. (1) are summarized, along with the experimental conditions, in Table 1. The length of the diffusion profiles varied between ~1000 and 3000 Å, depending on the experimental condition. The length of a profile at any specific temperature–time combination can be calculated from the diffusion data in Table 2 using the relation $x \sim 4(Dt)^{1/2}$, which follows from Eq. (1) by setting $C(x, t) = C_\infty$.

We also show in Fig. 1B the mol% of Cr in the octahedral site as a function of distance within the diffusion zone of olivine. These values were calculated from the ratio of the secondary ion intensities of Cr and Si, defined as I(Cr)/I(Si), the wt% of SiO_2 as determined from the microprobe analysis, and the sensitivity factor (F) of Cr relative to Si, according to

$$\text{wt\% } Cr_2O_3 = F\left(\frac{I(\mathrm{Cr})}{I(\mathrm{Si})}\right)(\text{wt\% } SiO_2). \quad (2)$$

The parameter F was calculated from the secondary ion intensities of Cr and Si beyond the diffusion zone and the Cr_2O_3 and SiO_2 contents in this zone (Table 1). The wt%Cr_2O_3 was then converted to mol% Cr in the octahedral site.

To check if the retrieved diffusion coefficient at a fixed temperature and fO_2 condition depended on the duration of the experiment, in which case there would have been interference from non-diffusive transport processes, we conducted time-series experiments at 900 and 1000 °C. The results, which are illustrated Fig. 2, do not show any

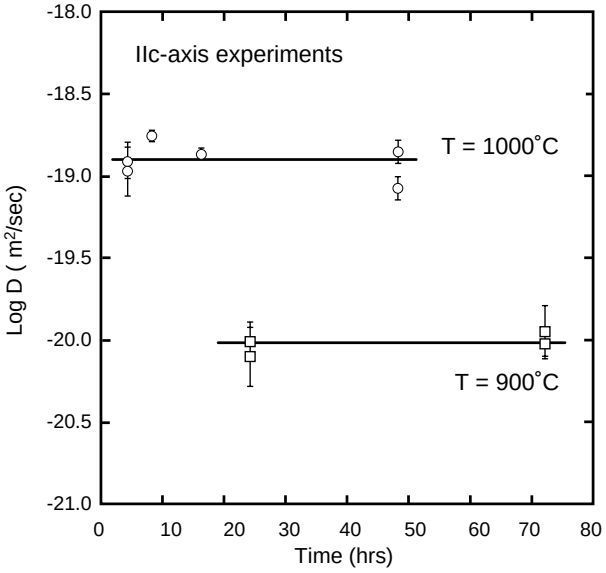

Fig. 2. Time series experiments of Cr diffusion parallel to the *c*-axis in olivine at 1 bar, 900 and 1000 °C.

time dependence of the retrieved diffusion coefficients. The D value at a given condition was calculated from the data of the best quality diffusion profile. The standard deviation (σ) of a D value resulting from the scatter of the data is represented by a vertical bar ($\pm\sigma$), and was calculated according to the method of Tirone et al. (2005).

The results for Cr diffusion in olivine at fO_2 conditions defined by the WI buffer are presented in Table 1, and plotted as Arrhenian relations for diffusion parallel to the a- and c-axis in Fig. 3. It is clear that there is significant diffusion anisotropy of Cr in olivine. With the Arrhenian equation expressed as $D = D_o \exp(-E/RT)$, where E is the activation energy and R is the gas constant, the data illustrated in Fig. 3 yield

$$\begin{aligned} \log D_o(||a) &= -5.31 \pm 0.39 \text{ m}^2 \text{ s}^{-1}; \\ E(||a) &= 352 \pm 10 \text{ kJ mol}^{-1} \\ \log D_o(||c) &= -6.65 \pm 0.59 \text{ m}^2 \text{ s}^{-1}; \\ E(||c) &= 299 \pm 14 \text{ kJ mol}^{-1}, \end{aligned} \quad (3)$$

where the uncertainties represent $\pm 1\sigma$ (1 standard deviation), and account for the errors of the retrieved D values (Table 1). Fig. 3 also shows $\pm 1\sigma$ errors of the $\log D$ values at selected temperatures, using the retrieved Arrhenian parameters above. These errors were calculated according to Tirone et al. (2005) taking into account the co-variance of the errors. On the basis of the earlier studies on cation diffusion in olivine (e.g., Buening and Buseck, 1973; Misener, 1974; Morioka and Nagasawa, 1991; Chakraborty et al., 1994), we expect the Cr diffusion parallel to the b axis to be intermediate between those parallel to the a- and c-axes.

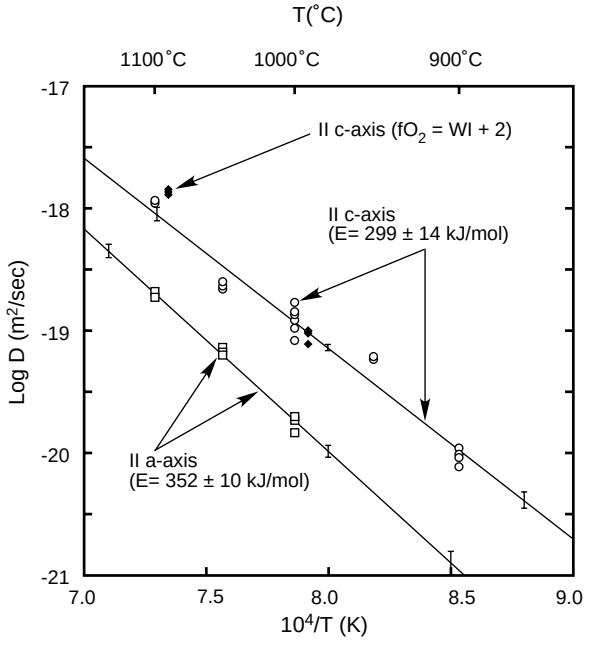

Fig. 3. Arrhenius plot of diffusion coefficients of ^{52}Cr in olivine. Open symbols, fO_2 of WI buffer; circles, D $\|$ c-axis; squares, D $\|$ a-axis; solid diamonds (slightly displaced for clarity): D $\|$ c-axis and fO_2 = two log units above WI buffer. The solid lines are least squares fits to the experimental data. The vertical lines on the least squares fit represent error bars of $\pm 1\sigma$.

The diffusion coefficients parallel to the c-axis that were obtained from annealing experiments at 1000 and 1100 °C, 1 bar, $\log fO_2 = WI + 2$ (Table 2) are illustrated in Fig. 3 by filled symbols (WI + 2 means two log units above the fO_2 defined by the wüstite–iron buffer condition). These results do not show any change of D(Cr) for a change of fO_2 by a factor of 100. In contrast, Fe^{2+}–Mg interdiffusion kinetics in olivine have been found to vary approximately as $fO_2^{1/6}$ (Buening and Buseck, 1973; Misener, 1974; Nakamura and Schmalzried, 1984). The lack of any detectable effect of the change of fO_2 condition on D(Cr) may suggest an extrinsic mechanism of Cr^{3+} diffusion in olivine in which the vacancy concentration was primarily controlled by the heterovalent substitution of Cr^{3+} according to $2Cr^{3+} + V(M)^{VI} = 3\,M^{2+}$, where $V(M)^{VI}$ stands for a vacancy in the octahedral M^{2+} cation site. By implication, it means that the vacancy concentration created by the process of homogeneous oxidation of Fe^{2+} was too small compared to that needed for the vacancy mediated diffusion of Cr^{3+}.

Tsai and Dieckmann (2002) have presented a detailed study of point defects or lattice vacancies in olivine formed by the homogeneous oxidation of octahedral Fe^{2+} ($V(Fe)^{VI}$ for brevity) as function of fO_2, T and $X_{Fe}{}^{2+}$. Using their data and relationship between the activities of octahedral vacancy $a_{v(Fe)}{}^{VI}$ and Fe^{3+}, we obtain, $a_{v(Fe)}{}^{VI}$, ($T \sim 1100$ °C) $\approx 4 \times 10^{-5}$. If we assume that the vacancies mix within the octahedral site without significant deviation from ideality, that is $X_{v(Fe)}{}^{VI} \approx a_{v(Fe)}{}^{VI}$, then the data in Fig. 1B indicate that $X_{v(Fe)}{}^{VI} \sim 10$–20 times $X_{Cr}{}^{VI}$ within the diffusion zone. This would seem to contradict the suggestion of extrinsic mechanism and favor an interstitial mechanism for the diffusion of Cr^{3+} in olivine. However, since the concentrations of both Cr^{3+} and octahedral vacancies are very dilute, the probability of finding $V(Fe)^{VI}$ and Cr^{3+} ions adjacent to one another could be too small for these vacancies to be effective for diffusion of Cr^{3+}. In that case the extrinsic mechanism would be a viable mechanism for the diffusion of Cr^{3+} despite the fact that $X_{v(Fe)}{}^{VI} > X_{Cr}{}^{VI}$. Clearly, further work is needed to understand the reason for the lack of effect of fO_2 change between WI and WI + 2 on the D(Cr).

Fig. 4 shows a comparison of the data for Cr tracer diffusion, as determined in this work, with those of Fe–Mg interdiffusion (Chakraborty, 1997), Ni tracer diffusion (Petry et al., 2004) and O diffusion (Ryerson et al., 1989) in olivine at specified fO_2 conditions. All cation diffusion data are for diffusion parallel to the c-axis. The activation energy for diffusion at fO_2 condition that varies along a solid buffer is ~36 kJ/mol larger than that for diffusion at constant fO_2 condition (Chakraborty and Ganguly, 1991).

4. Closure-temperature and -age of Mn–Cr system in olivine

Closure temperature (T_c) of a decay system in a mineral is defined to be the temperature at which diffusion of the

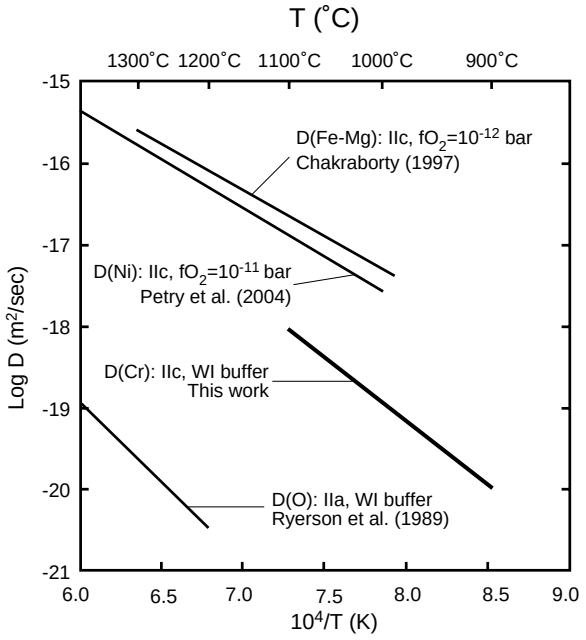

Fig. 4. Comparison of some cation and oxygen diffusion data in olivine. D(Fe–Mg): Fe–Mg interdiffusion data at Fe/(Fe + Mg) = 0.86 (Chakraborty, 1997); D(Ni): Ni self diffusion data (Petry et al., 2004), and D(O): Oxygen self diffusion data (Ryerson et al., 1989). All cation diffusion data are for diffusion parallel to c-axis whereas D(O) is for that parallel to a-axis.

daughter product had effectively ceased during cooling, thus enabling a record of elapsed time since T_c by the geochronological clock. Dodson (1973, 1986) formalized the concept of closure temperature in mathematical terms and derived a simple expression for the calculation of T_c which has been used extensively in the literature. The classic Dodson formulation assumed that there was sufficient diffusion in the mineral prior to the T_c that led to significant change in the concentration of daughter product at any part of the mineral. Ganguly and Tirone (1999) extended this formulation to remove the assumption of diffusive loss such that one can calculate the closure temperature of a decay system for any arbitrary loss of the daughter product. The modified formulation is

$$\frac{E}{RT_c} = \ln\left(-\frac{A'RT_c^2 D_o}{E(\mathrm{d}T/\mathrm{d}t)_{@T_c}a^2}\right), \tag{4}$$

where $(\mathrm{d}T/\mathrm{d}t)_{@T_c}$ is the cooling rate at T_c, a is a characteristic dimension of the mineral grain (radius for sphere and cylinder and half-length for plane sheet) and A' is a function of the grain geometry, cooling rate, diffusion coefficient at the peak or initial temperature, $D(T_o)$, at which the grain had a uniform distribution of the daughter product prior to the onset of cooling, and a. The above expression of T_c is the same as Dodson's except that in the latter, A' is replaced by A which depends only on the geometric factor. The function A' can be expressed as $\exp(G+g)$, where G represents a geometric factor, with values of 4.0066 for sphere, 3.29506 for cylinder and 2.15821 for plane sheet (Dodson, 1973), and g is a function of all the other variables listed above for A'. The values of g as function of a dimensionless parameter, M, that incorporates cooling rate, grain size, $D(T_o)$ and activation energy, were presented in graphical form by Ganguly and Tirone (1999) and in tabular form by Ganguly and Tirone (2001).

The cooling was assumed to have followed an asymptotic law that is given by

$$\frac{1}{T} = \frac{1}{T_o} + \eta t, \tag{5}$$

so that $\mathrm{d}T/\mathrm{d}t = -\eta T^2$, where η is a cooling time constant (with dimension of $\mathrm{K}^{-1}\,\mathrm{t}^{-1}$). Consequently, the term $T_c^2/(\mathrm{d}T/\mathrm{d}t)$ in Eq. (4) may be replaced by $-1/\eta$. The closure temperature in a given mineral grain can vary as function of distance from the center, depending in the size of the grain and the diffusivity of the daughter product, in which case Eq. (4) yields a weighted average over the entire grain. When $T_c = f(x)$ where x is the distance from the center, one can also calculate $T_c(x)$ by treating A' as function of x (Dodson, 1986; Ganguly and Tirone, 1999, 2001).

Fig. 5 shows the T_c of Cr in olivine as function of cooling rate and grain sizes, as calculated according to Eq. (4) using the diffusion data parallel to a- and c- axis. Fig. 6 illustrates T_c as function of a dimensionless variable, M, for T_o of 900, 1000, and 1100 °C, as calculated according to Eq. (4) and the classic Dodson formulation (Dodson, 1973). M is defined as

$$M = \frac{RD(T_o)}{E\eta a^2}, \tag{6}$$

where $D(T_o)$ is the diffusion coefficient at T_o. The parameter $\sqrt{M}$ can be viewed as the effective diffusion distance, which depends on the diffusion coefficient and cooling rate, normalized to the characteristic size the grain. It is evident from Fig. 6, and as also emphasized by Ganguly and Tirone (1999), the commonly used Dodson formulation (Dodson, 1973) is valid only for $\mathrm{Log}\sqrt{M} > -0.5$.

Within a single grain, the closure temperature is variable and progressively decreases towards the rim, thereby leading to an age profile (Dodson, 1986; Ganguly and Tirone, 1999). Fig. 7 shows a Mn–Cr age profile, which would develop in olivine grains upon cooling according to the asymptotic relation such that the cooling rate at 1000 °C is 5 °C/Myr, as calculated according to Ganguly and Tirone (1999). The age profiles are presented in terms of the extent of resetting of age (Δt) as a function of the normalized radial distance (r/a) from the center and the dimensionless parameter M. A horizontal dashed line indicates the average resetting of the age of a grain corresponding to the age profile to which it is connected.

As an illustration of the use of Fig. 7, let us consider the age profiles that would develop in spherical grains for a cooling rate of 5 °C/Myr at 1000 °C (i.e., $\eta = 3.08\times10^{-6}$ $\mathrm{K}^{-1}\mathrm{Myr}^{-1}$) for M values of 1.37, 0.34, and 0.07. If $T_o = 1000$ °C, then $D(T_o) = 1.2\times10^{-19}\,\mathrm{m}^2\,\mathrm{s}^{-1}$. Conse-

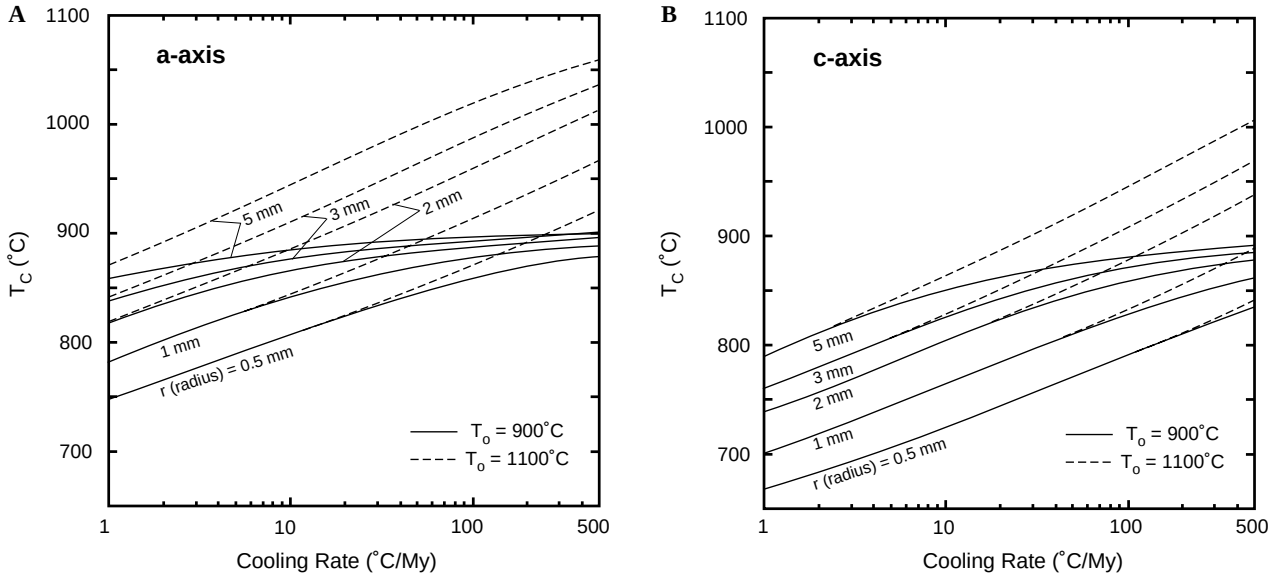

Fig. 5. Closure temperature (T_c) of Cr diffusion in olivine as a function of the initial temperature (T_o), cooling rate and grain size for diffusion parallel to (A) *a*-axis and (B) *c*-axis.

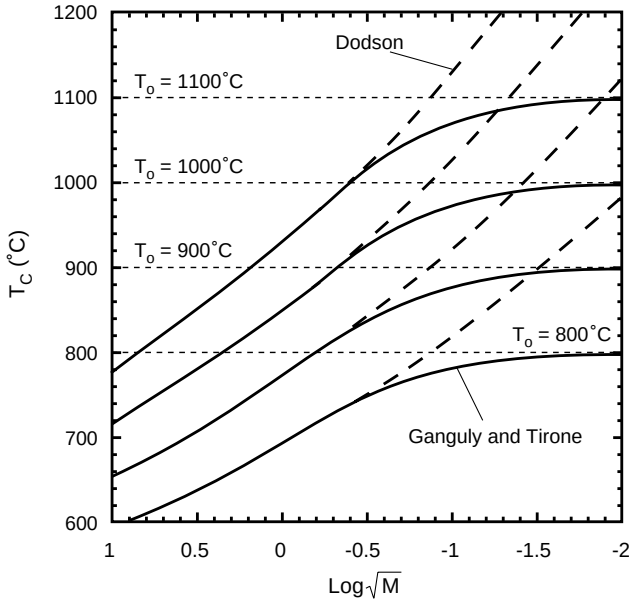

Fig. 6. Closure temperature (T_c) for spherical grain as function of the dimensionless variable $\sqrt{M}$, which is a measure of the effective diffusion distance normalized to the grain size Eq. (6). Dashed lines: Dodson formulation (1973); solid lines: modified Dodson formulation by Ganguly and Tirone (1999). The range of Log$\sqrt{M}$ value corresponds to cooling rates of 5–100 °C/Myr and grain radius of 1–5 mm.

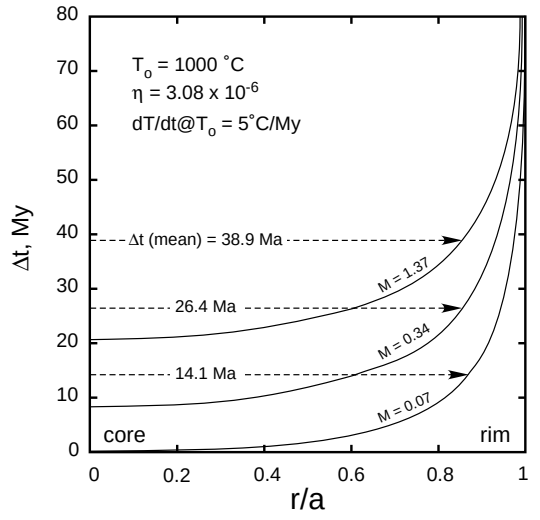

Fig. 7. Resetting of Mn–Cr age (Δt) in olivine single crystal during cooling as a function of the dimensionless parameter, M Eq. (6), and normalized distance, using a T–t path defined by an asymptotic cooling model Eq. (5) with $\eta = 3.08 \times 10^{-6}$ $K^{-1}Myr^{-1}$, corresponding to a cooling rate of 5 °C/Myr at 1000 °C.

quently, from Eq. (6), a (radius) = 5, 10, 23 mm. In other words, if $T_o = 1000$ °C, and the cooling rate at 1000 °C is 5 °C/Myr and defined by Eq. (5), then the three age profiles shown in Fig. 7 would develop in spherical grains with the above radii in the order of decreasing M values. These calculations afford a practical guide to geochronologists who abrade mineral grains to remove the marginal portions that might have reset during cooling (e.g., Lugmair and Shukolyukov, 1998), and in the choice of grain size that had preserved the peak age in the central portion ($M \geqslant 0.07$).

5. ^{53}Mn–^{53}Cr Thermochronology of olivine

5.1. Formulation of the thermochronological method

Applying the concept of age profile (Fig. 7), Ganguly and Tirone (2001) and Ducea et al. (2003) have shown that one can directly retrieve the cooling rate from the difference

between the average age of a central segment and that of the whole grain using a single decay system. Ganguly et al. (1998b) also developed an alternative method of determining the cooling rate from the average cooling age of garnet, as determined by the Sm–Nd decay system, when the extent of resetting of the average Sm–Nd age during cooling is known. Here, we present an extension of the second method to the ^{53}Mn–^{53}Cr system in olivine, and apply it calculate the cooling rate of a pallasite.

The method of Ganguly et al. (1998b) to determine the cooling rate from the bulk cooling age is based on the fact that any point on the curve of average T_c vs cooling rate for a specific grain size (Fig. 5) defines an elapsed time (Δt) between T_o and T_c. Thus given T_o and grain size, one can find the point on the appropriate T_c vs cooling rate curve that yields the observed value of Δt. This point then defines both T_c and the cooling rate at T_c, and hence η Eq. (4).

Fig. 8 shows a plot of $\log(\dot{T}a^2)$ vs. $\log(\Delta t/a^2)$ for different values of T_o, where $\dot{T}$ is the cooling rate at T_c. The axes variables have been chosen according to Ganguly et al. (1998a) to linearize the plots as much as possible. The curves were constructed using the average of the diffusion coefficients parallel to *a*- and *c*- axis of olivine. A vertical bar on a curve indicates the variation of the *Y*-axis value resulting from that of D(Cr) in olivine parallel to the slowest (*a*-axis) and fastest (*c*-axis) diffusion directions. The chosen range of T_o should encompass the range of temperatures of interest in the use of Mn–Cr decay system in the early solar system objects. The curves in Fig. 8 constitute graphical Mn–Cr thermochronmeters that could be used

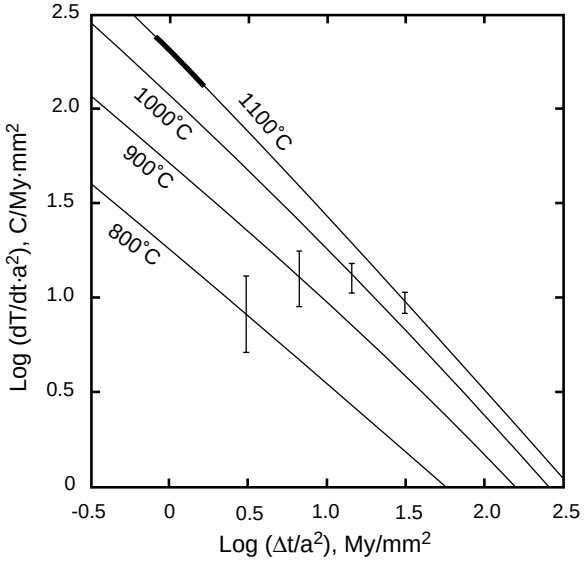

Fig. 8. Cooling rate of spherical olivine crystal (a: radius) as a function of the age loss or resetting (Δt) of the ^{53}Mn–^{53}Cr decay system and peak temperature (T_o), which are shown on the individual curves, using the average of diffusion coefficients parallel to the *c*- and *a*-axis. A vertical bar on a curve represents the variation of the *Y*-axis parameter corresponding to the variation of the diffusion coefficient between the two crystallographic directions. The thick segment on the 1100 °C isotherm indicates the data for Omolon pallasite.

to directly retrieve initial cooling rate from a knowledge of resetting of the Mn–Cr age of olivine, T_o and the average size of the olivine grains that were used to determine the age (computer programs are also available from the authors for these calculations).

5.2. Application to the cooling rate of a pallasite

Pallasites are stony-iron meteorites that consist mostly of olivines within a matrix of Fe–Ni alloys, and minor phases like troilite (FeS) and schreibersite (Fe_3P; Buseck, 1977). The mixing of olivine and metals are commonly interpreted to indicate the derivation of pallasites from near the core-mantle boundary of the parent body (e.g., Scott and Taylor, 1990). Pallasites contain both rounded and angular olivine grains, and have been classified into different textural types according to the presence of the rounded vs angular grains, and the microscopically rounded corners of the angular grains (Scott, 1977; Ohtani, 1983). The presence of angular olivine grains has been interpreted to be the result of fragmentation and excavation of the silicate mantle of the parent body by a giant impact, followed by mixing with the metal core, and insufficient annealing time (Scott, 1977; Saiki et al., 2003). The rounding of the olivine grains are thought to reflect prolonged annealing time. However, from experimental studies of the kinetics of rounding olivine grains in a Fe–Ni matrix, Saiki et al. (2003) concluded that the large rounded grains in the Brenham-type pallasites were unlikely to have been produced by prolonged annealing of angular olivine grains in a Fe–Ni matrix. Instead, these olivine grains seem to be igneous cumulates.

The cooling rate of pallasites has been problematic, but is important to the evaluation of the idea that pallasites are samples from the core-mantle boundary, and for the calculation of the size of parent body. Buseck and Goldstein (1969) used metallographic method to evaluate the cooling rate of 33 pallasites. Yang et al. (1997) proposed new empirical technique for pallasite cooling rates on the basis of the size of cloudy zone of metallic phases. A cloudy zone is found in the inner part of a zoned taenite rim, the outer part being clear, and consists of high-Ni island phase and low-Ni honeycomb phase. A cloudy zone is believed to be a product of spinodal decomposition. According to the results of the metallographic studies of Buseck and Goldstein (1969) and Yang et al. (1997), the cooling rates of pallasite were 1–8 °C/Myr that is indicative of a core-mantle provenance. On the other hand, Miyamoto and Takeda (1994) and Miyamoto (1997) reported very rapid cooing rate of three pallasites (Esquel, Imilac, and Yamato 8451), 20– 100 °C/y, on the basis of model fits to the chemical zoning profiles of Ca and Fe in olivine in terms linear cooling from a peak temperature of 1100 °C at which the olivine grains were supposed to have homogeneous compositions. The pallasites studied by Buseck and Goldstein (1969) included Esquel and Imilac, and those studied by Yang et al. (1997) included the latter. Thus, for the same

pallasites, the cooling rates obtained from modeling the compositional zoning of olivine are 7–8 orders of magnitude faster than those obtained from the application of metallographic methods. To reconcile the widely differing results on the retrieved values of cooling rates, Miyamoto (1997) suggested a two-stage cooling history, in which the pallasites cooled very rapidly at high temperature, and then cooled very slowly at low temperatures to form the metallographic textures (Widmanstätten pattern) that are indicative of slow cooling.

Miyamoto (1997) modeled the compositional zoning of Fe on the basis of the Fe–Mg interdiffusion data, D(Fe–Mg), from Buening and Buseck (1973). These data are in strong disagreement with the data of Chakraborty (1997). Liermann and Ganguly (2002) evaluated the different sets of diffusion data on the basis of their experimentally determined D(Fe–Mg) data in spinel, and relative diffusivities of olivine and spinel as suggested from observations of the lengths of Fe–Mg compositional zoning in coexisting olivine and spinel (Ozawa, 1984). Their analysis strongly supports the diffusion data of Chakraborty (1997). Modeling of the data of Miyamoto (1997) on the basis of the D(Fe–Mg) values from Chakraborty (1997) and fixed edge composition yields cooling rates that are slower than those inferred by Miyamoto (1997) by a factor of $\sim(2\text{–}7)\times10^3$. Because of changing edge composition during cooling, the true cooling rate should be even slower. In addition, the compositional data of olivine near the margin, as given by Miyamoto (1997), are so highly scattered that cooling rates that are still slower by a factor of 5 are compatible with the data. From these considerations, we conclude that olivine zoning data presented by Miyamoto are compatible with cooling rates of ~2000 °C/Myr. Much better quality compositional data is needed to arrive at a more definitive conclusion about the cooling rates recorded by the compositional zoning in olivine. Nonetheless, it seems that there is probably a significant difference between the cooling rates suggested by the olivine zoning and metallographic data.

In this work, we determined the cooling rate of the pallasite Omolon on the basis of resetting of the Mn–Cr age of olivines, as determined by Lugmair and Shukolyukov (1998). The olivine crystals are partly rounded, sometimes with preserved crystal faces. There is no evidence of fragmentation (Lugmair, personal communication). Since Cr diffusion in olivine is slower than that of Fe–Mg interdiffusion (Chakraborty, 1997), the cooling rate obtained from the resetting of Mn–Cr age of olivine would reflect cooling rate above the closure temperature of Fe–Mg interdiffusion in olivine. According to Lugmair and Shukolyukov (1998), the bulk Mn–Cr age of olivine in this pallasite is 4558 ± 1.0 Ma, which is ~10 Myr younger than the age of the solar system. The forsterite content of the olivines in pallasites is ~90% (Miyamoto, 1997), which is similar to the composition of the olivine grains used in our study. Thus, we could directly use the graphical relationship presented in Fig. 8 to calculate the cooling rate of Omolon, using reasonable assumptions for some of the unknown parameters.

Brett and Sato (1984) measured the fO_2 of several meteorites. According to their study, the fO_2 values of Pallasite and E-Chondrite are three orders of magnitude below WI buffer. Usually, the diffusion coefficient of an atom in ferromagnesian mineral changes with fO_2. However, our experimental data did not show any effect of fO_2 on the Cr^{3+} diffusion coefficient in olivine in the range of fO_2 between WI and two orders of magnitude above the WI buffer condition. We, thus, assume that the D(Cr) in olivine determined in this work is applicable to the pallasites as well.

The olivine grains analyzed by Lugmair and Shukolyukov (1998) were around ~5 mm in diameter, and the estimated loss due to etching prior to the mass spectrometric analysis was ~0.01 mm (Lugmair, personal communication). It should be clear from Fig. 7 that the resetting of Mn–Cr age of olivine, as determined from the etched grains, should be very similar to that of the original grains. Now, the cooling rate that we intend to calculate is in the parent body of pallasites, for which we need to know the time between the formation of the parent body and the formation of the solar system. We assume this to be 0–5 Myr. A value of 3 Myr is preferred by Lugmair (personal communication). Thus, the age loss (Δt) of the Mn–Cr system in olivine in Omolon since the parent body formation is <10 Myr, and probably within ~10–5 Myr. Miyamoto (1997) used a peak temperature of 1100 °C for pallasites. Using $T_o = 1100$ °C, $\Delta t = 10\text{–}5$ Myr and $a = 2.5$ mm, we obtain from Fig. 8 average cooling rate of ~20–40 °C/Myr between 1100 °C and T_c. The latter can be calculated according to the relation $T_c = T_o - (dT/dt)(\Delta t)$, which yields $T_c \approx 985\text{–}1000$ °C.

Since the cooling rate depends on temperature, and we have retrieved an average cooling rate between T_o and T_c, we assume that the cooling rate applies to the mean temperature between T_o and T_c, and thus calculate the cooling time constant, η, to be $(1.7\text{–}2.8)\times10^{-5}$/K-Myr from Eq. (5). The metallographic cooling rate applies to the temperature range of 300–700 °C (e.g., Miyamoto, 1997). If the cooling of Omolon parent body is assumed to have followed the asymptotic form of Eq. (5), then the inferred value of η yields cooling rate of 10–17 °C/Myr at 500 °C, which is in good agreement with the metallographic cooling rate. We, thus, conclude that the pallasite Omolon had underwent smooth cooling within the parent body rather than a two-stage cooling, as suggested by Miyamoto. Also since the samples are not fractured, it seems reasonable to conclude that the excavated sample represents a material from the core/mantle boundary.

Wood (1979) calculated, with and without heat production from the decay of ^{26}Al, the size of parent body of meteorite and the depth of burial of an excavated sample as function of T_o and the cooling rate at 500 °C. He assumed T_o of 1000 and 600 °C. Comparison of the results

for these two T_o values suggest that the inferred size of the parent body and burial depth of Omolon would not be significantly affected from those calculated using T_o of 1000 °C even if the actual T_o had differed by ~100 °C. Using Wood's calculation, we thus infer a burial depth of ~30 km for the pallasite Omolon in a parent body of at least ~100 km radius.

Acknowledgments

This research was supported by NASA Grants NAG5-7364 and NNG04GG26G, and a post-doctoral fellowship for research abroad to M.I. from the Japan Society for the Promotion of Sciences. Thanks are due to Prof. Richard Hervig for access to the Ion probe laboratory of the Arizona State University and advice, Dr. Marilena Stimpfl for orientating the olivine crystals, and to Prof. Gunter Lugmair for discussion about the Omolon pallasite. We greatly appreciate the constructive reviews of Prof. David Kohlstedt, Dr. Jim Van Orman, and Dr. Rick Ryerson. Prof. Kohlstedt and Dr. Van Orman independently suggested the possibility of extrinsic mechanism for Cr diffusion in olivine. Thanks are due to Prof. Sumit Chakraborty for discussions about defect chemistry of olivine.

Associate editor: F.J. Ryerson

References

Brett, R., Sato, M., 1984. Intrinsic oxygen fugacity measurements on seven chondrites, a pallasite, and a tektite and the redox state of meteorite parent body. *Geochim. Cosmochim. Acta* **48**, 111–120.

Buening, D.K., Buseck, P.R., 1973. Fe–Mg lattice diffusion in olivine. *J. Geophy. Res.* **78**, 6852–6862.

Buseck, P.R., 1977. Pallasite meteorites—mineralogy, petrology and geochemistry. *Geochim. Cosmochim. Acta* **41**, 711–721.

Buseck, P.R., Goldstein, J.I., 1969. Olivine compositions and cooling rates of pallasitic meteorites. *Geol. Soc. Am. Bull.* **80**, 2141–2158.

Chakraborty, S., 1997. Rates and mechanisms of Fe–Mg interdiffusion in olivine at 980–1300 °C. *J. Geophy. Res.* **102** (B6), 12317–12331.

Chakraborty, S., Farver, J.R., Yund, R.A., Rubie, D.C., 1994. Mg tracer diffusion in synthetic forsterite and San Carlos olivine as a function of P, T and fO_2. *Phys. Chem. Minerals* **21**, 489–500.

Chakraborty, S., Ganguly, J., 1991. Compositional zoning and cation diffusion in garnet. In: Ganguly, J. (Ed.), *Diffusion, Atomic ordering and mass transport. Advances in Physical Geochemistry*, Vol. 8. Springer-Verlag, Berlin, pp. 120–175.

Crank, J., 1975. *The Mathematics of Diffusion*, second ed., Oxford University Press.

Dodson, M.H., 1973. Closure temperature in cooling geochronological and petrological systems. *Contrib. Mineral. Petrol.* **40**, 259–274.

Dodson, M.H., 1986. Closure profiles in cooling systems. In: Dennis, P.F., Freer, R. (Eds.), *Kinetics and Transport in Silicate and Oxide Systems*, Materials Science Forum, 7, *Min. Soc.* Great Britain, pp. 145–155.

Ducea, M., Ganguly, J., Rosenberg, E., Patchett, P.J., Cheng, W., 2003. Sm–Nd dating of spatially controlled domains of garnet single crystal: a new method of high temperature thermochronology. *Earth Planet. Sci. Lett.* **213**, 31–42.

Ganguly, J., Cheng, W., Chakraborty, S., 1998a. Cation diffusion in aluminosilicate garnets: experimental determination in pyroxene-almandine diffusion couples. *Contrib. Mineral. Petrol.* **131**, 171–180.

Ganguly, J., Tirone, M., Hervig, R.L., 1998b. Diffusion kinetics of Samarium and Neodymium in Garnet, and a method for determining cooling rates of rocks. *Science* **281**, 805–807.

Ganguly, J., Tirone, M., 1999. Diffusion closure temperature and age of a mineral with arbitrary extent of diffusion: theoretical formulation and applications. *Earth Planet. Sci. Lett.* **170**, 131–140.

Ganguly, J., Tirone, M., 2001. Relationship between cooling rate and cooling age of a mineral: theory and applications to meteorites. *Meteor. Planet. Sci.* **36**, 167–175.

Hutcheon, I., Krot, A.N., Keil, K., Phinney, D.L., Scott, E.R.D., 1998. ^{53}Mn–^{53}Cr dating of fayalite formation in the CV3 chondrite mokoia: evidence for asteroidal alteration. *Science* **282**, 1865–1867.

Ito, M., Ganguly, J., 2004. Potassium diffusion in melilite: experimental studies and constraints on the thermal history and size of planetsimals hosting CAIs. *Meter. Planet. Sci.* **39**, 1911–1919.

James, F., Roos, M., 1975. MINUIT—a system for function minimization and analysis of the parameter errors and correlations. *Comput. Phys. Commun.* **10**, 343–367.

Liermann, H-P., Ganguly, J., 2002. Diffusion kinetics of Fe and Mg in aluminous spinel: experimental determination and applications. *Geochim. Cosmochim. Acta* **66**, 2903–2913.

Lugmair, G.W., Shukolyukov, A., 1998. Early solar system timescales according to ^{53}Mn–^{53}Cr systematics. *Geochim. Cosmochim. Acta* **62**, 2863–2886.

Misener, D.J., 1974. Cationic diffusion in olivine to 1400 °C and 35 kbar. In: Hofmann A.W. et al. (Eds.), *Geochemical Transport and Kinetics.*/ Carnegie Inst. Wash. Publ., 634/. Washington DC: Carnegie Inst., 117–129.

Miyamoto, M., 1997. Chemical zoning of olivine in several pallasites. *J. Geophy. Res.* **102** (No. E9), 21613–21618.

Miyamoto, M., Takeda, H., 1994. Chemical zoning of olivine in several pallasites suggestive of faster cooling. *Lunar Planet. Sci.* **XXV**, 921–922.

Morioka, M., Nagasawa, H., 1991. Ionic diffusion in olivine. In: Ganguly, J. (Ed.), *Diffusion, Atomic Ordering and Mass Transport. Advances Physical Geochemistry*, Vol. 8. Springer, New York, pp. 176–197.

Nakamura, A., Schmalzried, H., 1984. On the Fe^{2+}–Mg^{2+}-interdiffusion in olivine (II). *Ber. Bunsenges. Phys. Chem.* **88**, 140–145.

Nyquist, L., Lindstrom, D., Mittlefehldt, D., Shih, S.-H., Wiesmann, H., Wentworth, S., Martinez, R., 2001. Manganese-chromium formation intervals for chondrules from the Bishunpur and Chainpur meteorites. *Meteor. Planet. Sci.* **36**, 911–938.

Ohtani, E., 1983. Formation of olivine textures in pallasites and thermal history of pallasites in their parent body. *Phys. Earth Planet. Inter.* **32**, 182–192.

Ozawa, K., 1984. Olivine–spinel geospeedometry: analysis of diffusion-controlled Mg–Fe^{2+} exchange. *Geochim. Cosmochim. Acta* **48**, 2597–2611.

Petry, C., Chakraborty, S., Palme, H., 2004. Experimental determination of Ni diffusion coefficients in olivine and their dependence on temperature, composition, oxygen fugacity, and crystallographic orientation. *Geochim. Cosmochim. Acta* **68**, 4179–4188.

Ryerson, F.J., Durham, W.B., Cherniak, D.J., Lanford, W.A., 1989. Oxygen diffusion in olivine: effect of oxygen fugacity and implications for creep. *J. Geophys. Res.* **94**, 4105–4118.

Scott, E.R.D., 1977. Formation of olivine-metal textures in pallasite meteorites. *Geochim. Cosmochim. Acta* **41**, 693–710.

Scott, E.R.D., Taylor, G.J., 1990. Origins of pallasites at the core-mantle boundaries of asteroids. *Lunar Planet. Sci.* **XXI**, 1119–1120.

Saiki, K., Laporte, D., Vielzeuf, D., Nakashima, S., Boivin, P., 2003. Morphological analysis of olivine grains annealed in an iron-nickel matrix: experimental constraints on the origin of pallasites and on the thermal history of their parent bodies. *Meter. Planet. Sci.* **38**, 427–444.

Sugiura, N., 2002. Mn–Cr chronology of olivine in some meteorites. *Lunar Planet. Sci.* **XXXIII**, CD-ROM#1435.

Tirone, M., Ganguly, J., Dohmen, R., Langehorst, F., Hervig, R., Becker, H-W., 2005. Rare earth diffusion kinetics in garnet: experimental studies and applications. *Geochim. Cosmochim. Acta* **69**, 2385–2398.

Tsai, T.-L., Dieckmann, R., 2002. Variation of the oxygen content and point defects in olivines, $(Fe_x–Mg_{1-x})_2SiO_4$, $0.2 \leqslant x \leqslant 1.0$. *Phys. Chem. Minerals* **29**, 680–694.

Yang, C.-W., Williams, D.B., Goldstein, J.I., 1997. A new empirical cooling rate indicator for meteorites based on the size of the cloudy zone of the metallic phases. *Meteor. Planet. Sci.* **32**, 423–429.

Wood, J.A., 1979. Review of the metallographic cooling rates of meteorites and a new model for the planetesimals in which they formed. In: Gehrels, T. (Ed.), *Asteroids*. University of Arizona Press, pp. 849–891.